Real-time imaging of laser-induced membrane disruption of a living cell observed with multifocus coherent anti-Stokes Raman scattering microscopy

Takeo Minamikawa,[a] Hirohiko Niioka,[b] Tsutomu Araki,[a] and Mamoru Hashimoto[a]
[a]Osaka University, Graduate School of Engineering Science, Toyonaka Osaka 560-8531, Japan
[b]Osaka University, Institute for Nanoscience Design, Toyonaka, Osaka 560-8531, Japan

Abstract. We demonstrate the real-time imaging of laser-induced disruption of the cellular membrane in a living HeLa cell and its cellular response with a multifocus coherent anti-Stokes Raman scattering (CARS) microscope. A near-infrared pulsed laser beam tightly focused on the cellular membrane of a living cell induces ablation at the focal point causing a local disruption of the cellular membrane. After the membrane disruption a dark spot decreasing CARS intensity of 2840 cm^{-1} Raman shift at the disrupted site appears. This dark spot immediately disappears and a strong CARS signal is observed around the disrupted site. This increase of the CARS signal might be caused by resealing of the disrupted site via aggregation of the patch lipid vesicles in the cytoplasm. The accumulation of lipids around the disrupted site is also confirmed with three-dimensional CARS images of a cell before and after membrane disruption. The temporal behavior of the CARS signal at the disrupted site is observed to detect the fusion dynamics of patch vesicles. [DOI: 10.1117/1.3533314]

Keywords: coherent anti-Stokes Raman scattering microscopy, multifocus excitation, laser-induced membrane disruption, membrane resealing, living cell.

Paper 10301SSPR received Jun. 1, 2010; revised manuscript received Sep. 30, 2010; accepted for publication Oct. 15, 2010; published online Feb. 14, 2011.

1 Introduction

Laser-assisted modification, dissection, and trapping of a single cell and its organelles are effective techniques for analyzing the characteristics of the cell because of their ability to make noncontact but direct access to intracellular organelles.[1–9] Manipulation of cells by these techniques has been studied using several imaging methods, such as electron microscopy,[10,11] differential interference contrast (DIC) microscopy,[12] and fluorescence microscopy,[12–14] Although electron microscopy reveals the nanometer-scale morphological structure of the manipulated site, time-resolved imaging of a manipulated living cell is difficult because of the requirement for sample preparation steps, such as fixation and dehydration. On the other hand, DIC microscopy enables real-time observation with submicrometer spatial resolution without any sample preparation; however, molecular species and structures cannot be distinguished. Fluorescence microscopy selectively visualizes molecular species of a cell by staining with fluorophores, and real-time imaging of living cells is also possible. Unfortunately, fluorophores are often photobleached in observation and sometimes affect cellular functions of a living cell.

Coherent anti-Stokes Raman scattering (CARS) microscopy is a label-free and three-dimensional chemical imaging technique based on intrinsic molecular vibrations of a specimen.[15,16] The molecular vibrations are very sensitive to molecular species and structures, and therefore, information about the molecular species and structures can be obtained via the molecular vibration without staining. Because the CARS signal is anti-Stokes–shifted emission, the signal is easily separated with Stokes-shifted fluorescence. CARS is a nonlinear optical phenomenon, and thus, the spatial resolution of a CARS microscope is higher than that of a spontaneous Raman scattering microscope. CARS microscopy is therefore a powerful tool for visualization of cellular molecules in particular lipids with the strong CH_2 vibrations,[17–20] and real-time imaging is also possible.[21,22]

In this study, the laser-induced disruption of the cellular membrane of a living HeLa cell was observed with a multifocus CARS microscope in real time. The resealing process around the disrupted site was visualized.

2 Materials and Methods

2.1 *Multifocus coherent Anti-Stokes Raman Scattering Imaging System*

The optical setup of the multifocus CARS microscopy system is illustrated in Fig. 1, which is a modified system used in our previous study.[22,23] The system consisted of two picosecond mode-locked Ti:sapphire lasers operating at different wavelengths (pulse duration of 5 ps, repetition rate of 80 MHz, Tsunami, Spectra-Physics, Mountain View, California), a high-precision pulse synchronization system,[24] an automatic pulse duration minimizing system,[25] a microlens array scanner (lens diameter of 0.58 mm, focal length of 11.6 mm, MLA1-DD, Nanophoton, Osaka, Japan), a modified inverted microscope (TE-200, Nikon, Tokyo, Japan), and an

Address all correspondance to: Mamoru Hashimoto, Machitaneyama 1–3, Toyonaka, Osaka 560-8531, Japan. Tel: 81 6 850 6216; Fax: 81 6 850 6212; E-mail: mamoru@me.es.osaka-u.ac.jp.

1083-3668/2011/16(2)/021111/5/$25.00 © 2011 SPIE

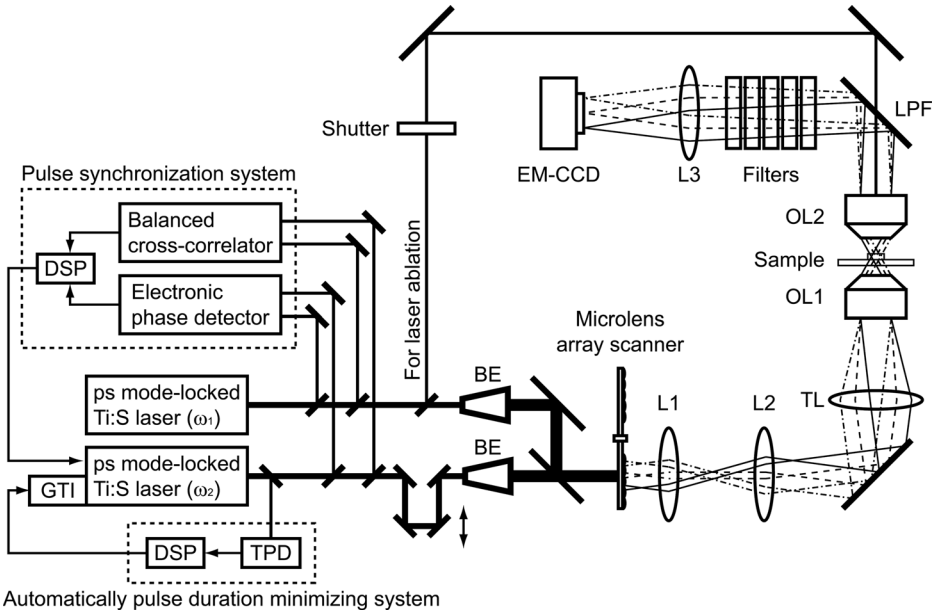

Fig. 1 Optical setup of the multifocus CARS microscopy system with near-infrared pulsed laser-induced ablation system (Ref. 23): L, lenses; BE, beam expander; TL, tube lens; OL, objective lenses; TPD, two-photon detector; DSP, digital signal processor; GTI, Gires-Tournois interferometer; LPF, long-wavelength-pass filter.

electron-multiplying charge-coupled device camera [(EM-CCD), DV-897, Andor, Belfast, United Kingdom].

The two laser pulses were synchronized with the high-precision pulse synchronization system and were spatio-temporally overlapped. The laser beams were made incident on the microlens array scanner to split them into multiple beamlets. The beamlets were collimated with relay lenses and focused to multiple spots on the specimen with an objective lens (OL1; S Fluor, Nikon, Tokyo, Japan, $\times 40$, (NA) = 0.85). The system produced 19 focal spots on the specimen from laser beams 4 mm in diameter. CARS signals from the multiple focal spots on the specimen were collected by another water-dipping objective lens (OL2; NIR Apo Nikon, Tokyo, Japan, $\times 60$, NA = 1.0), and the excitation beams were cut with optical filters. The CARS signals were observed in parallel with the EM-CCD camera, and a CARS image was obtained by rotating the microlens array disk. The wavelength of the lasers were tuned to 709 and 887 nm to excite CH_2 stretching vibration mode of lipids at 2840 cm^{-1}. The spatial resolution in the *xy* plane of the multifocus CARS microscopy system was determined by the diffractio limit for the wavelength of CARS emission because a two-dimensional image sensor was used. On the other hand, the spatial resolution along the *z*-axis was dependent on the excitation optics and the third-order nonlinearity of the CARS generation.

2.2 *Near-Infrared Picosecond Laser-Induced Ablation System*

Near-infrared pulsed laser-induced ablation has been used for less-invasive and spatially accurate surgery of a cell.[1] Near-infrared pulse laser light focused with a high-NA objective lens forms a submicrometer focal spot and causes ablation at the focal spot via a photoinduced ionization effect.[26] In our setup, part of the excitation laser light (709 nm) was used for laser ablation and was made incident on the microscope from the opposite direction to the CARS excitation laser beams through the water-dipping objective lens with NA = 1.0 (OL2). The intensity and exposure time for the laser ablation were controlled by a neutral density filter and a mechanical shutter, respectively.

2.3 *Sample Preparation*

HeLa cells were cultured in Dulbecco's modified Eagle's medium (GIBCO, Grand Island, New York) with 10% (v/v) fetal bovine serum and 1% (v/v) antibiotic/antimycotic solution (GIBCO, Grand Island, New York). For CARS imaging, HeLa cells were incubated on a glass-bottomed dish at 37°C in 5% CO_2 for 24 h, and then the culture medium was replaced with a modified Tyrode's solution (1 mM D-glucose, 145 mM NaCl, 1 mM $MgCl_2 \cdot 6H_2O$, 4 mM KCl, 10 mM HEPES, 1 mM $CaCl_2$, pH 7.4) or Ca-free Tyrode's solution (same as above omitting $CaCl_2$).

3 Results and Discussion

We obtained real-time CARS images of the cellular membrane disruption of a living HeLa cell induced by near-infrared laser ablation. Video 1 shows the real-time CARS images of a HeLa cell observed at 2840 cm^{-1}. As lipids have a strong Raman band of symmetric CH_2 stretching vibration at 2840 cm^{-1}, cellular membrane and organelles with lipids are visualized. The laser light for ablation was irradiated at 2 s in Video 1. The laser power and irradiation time used for ablation were 63.9 mW and 0.1 s, respectively. High-intensity plasma radiation was observed just after the laser irradiation. After the radiation, a dark spot and high CARS signal region appeared around the irradiated spot [Video 1(b)]. We thus concluded that the cellular membrane was disrupted with the laser irradiation. The dark spot immediately disappeared, but the high CARS signal remained for a few tens of seconds [Video 1(c)]. There are two

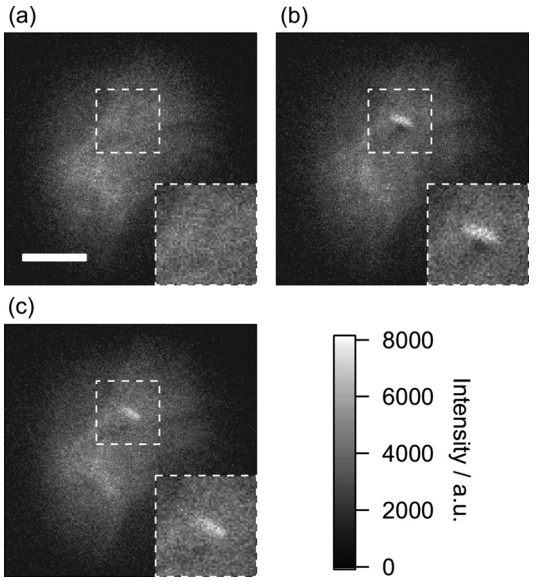

Video 1 Real-time CARS images of the laser-induced membrane disruption of a HeLa cell (a) before, (b) 1 s after, and (c) 2 s after ablation. The laser power and irradiation time used for ablation were 63.9 mW and 0.1 s, respectively. The observed molecular vibration was 2840 cm^{-1}. The image acquisition time was 0.2 s. The scale bar represents 20 μm. (QuickTime, 665 KB)
[URL: http://dx.doi.org/10.1117/1.3533314.1]

possibilities for forming the dark spot; one is forming a hole in the membrane that directly indicates the membrane ablation, the other one is a shade of laser-induced bubble that is induced after membrane ablation.[27] Both of these processes disrupt the membrane. The high CARS signal region was 2.5 times higher than that from other regions of the cellular membrane, indicating that the molecular density of lipids was increased after the disruption. We considered that the increase of the CARS signal was the result of lipid vesicle resealing of the disrupted site. When a cellular membrane is injured, lipid vesicles in the cytoplasm accumulate at the disrupted site to prevent Ca^{2+} entry because Ca^{2+} influx leads to cell death. This is known as the emergency response of the cell.[28]

The membrane resealing of a cell depends on Ca^{2+} concentration in the surrounding medium. In the absence of extracellular Ca^{2+}, the membrane resealing of a cell is not triggered.[28] To analyze Ca^{2+}-dependent membrane resealing, we obtained CARS images of a laser ablated HeLa cell in external Tyrode's solution without Ca^{2+} (Fig. 2). The laser power and irradiation time used for ablation were 68.3 mW and 0.1 s, which is the same condition in Video 1. The cellular membrane of the HeLa cell was ablated and disrupted by laser irradiation. A dark spot (700 nm in diameter) decreasing the CARS intensity appeared, but increase of CARS signal was not detected. The dark spot, however, remained at least for a few minutes in contrast with the Ca^{2+}-containing surrounding medium. The results indicates that the irradiating laser makes a hole of about a few micrometers in diameter. In this condition, the membrane resealing with lipid vesicles could occur if the Ca^{2+} were contained in the surrounding medium. This result supports the fact that the CARS signal increase in the presence of Ca^{2+} is caused by lipid resealing.

To confirm where the lipid vesicles accumulated, we observed three-dimensional images of the disrupted site in a HeLa cell before and after ablation. These are shown in Video 2. The

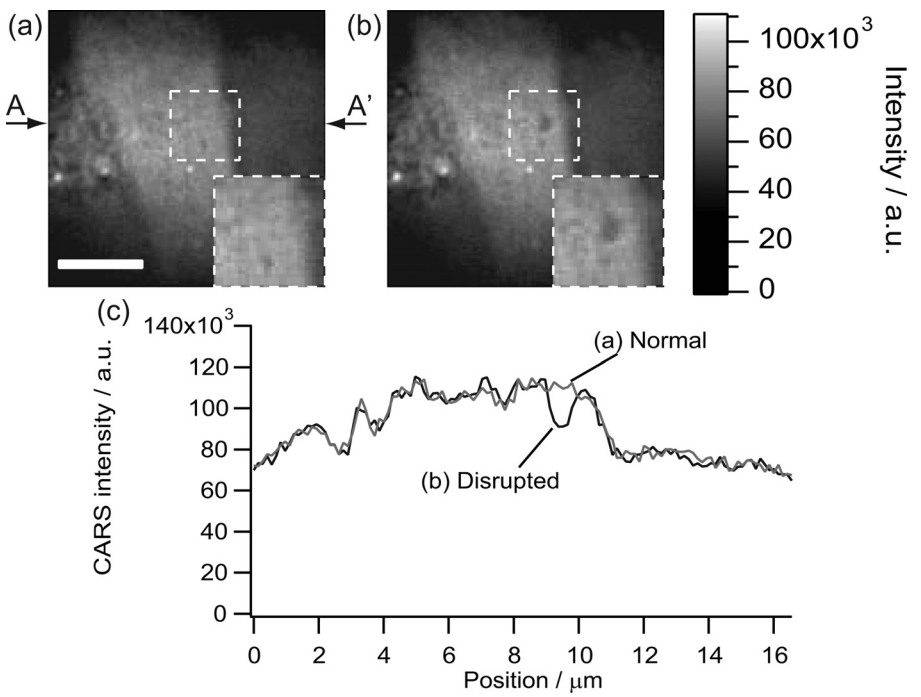

Fig. 2 CARS images of the disrupted site in a HeLa cell in extracellular Tyrode's solution that had no Ca^{2+}. CARS images of the laser-induced membrane disruption of a HeLa cell (a) before, (b) 1 min after ablation. (c) Cross-sectional line profile taken along the AA′ line indicated on the CARS images. The laser power and irradiation time used for ablation were 68.3 mW and 0.1 s, respectively. The observed molecular vibration was 2840 cm^{-1}. The image acquisition time was 10 s. The scale bar represents 5 μm.

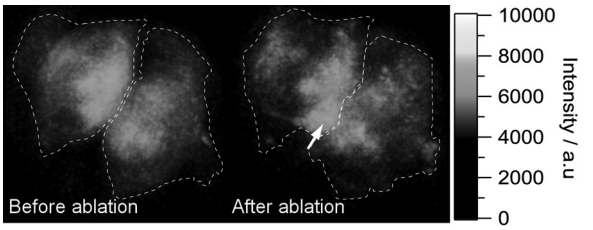

Video 2 Three-dimensional images of a HeLa cell (left) before and (right) after membrane ablation. The observed molecular vibration was 2840 cm^{-1}. The laser power and irradiation time used for ablation were 134mW and 0.1 s, respectively. There are two HeLa cells, and the membrane of the "before" HeLa cell was disrupted. The arrow indicates the disrupted site. The white dotted line indicates the boundary of the HeLa cells. (QuickTime, 601 KB)
[URL: http://dx.doi.org/10.1117/1.3533314.2]

laser power and irradiation time used for ablation were 134 mW and 0.1 s, respectively. The location of the disrupted site was confirmed with 2-D CARS imaging during the ablation. Three-dimensional images of the HeLa cell were constructed from z-sectioned CARS images obtained by moving the specimen in 500 nm steps with a piezoelectric stage. The acquisition time of each cross-sectional image was 500 ms. After the disruption, a CARS signal around the disrupted site was increased. The strong CARS signal indicates the accumulation of the lipid vesicles in the cytoplasm around the disrupted site due to the resealing. Because the irradiation laser power was higher than that of other experiments shown in Video 1 and Fig. 2, there was a great deal a of Ca^{2+} inflow into the cell. Therefore, a large amount of vesicles in order to stop the Ca^{2+} influx was gathered and the strong CARS signal region was observed inside of the cell.

We also observed the temporal behavior of the CARS signal at the disrupted site after ablation (Fig. 3). The signal was obtained from a pixel of the CARS images at the disrupted site with a frame rate of 5 fps. The laser light for ablation was irradiated at 2 s. The laser power and irradiation time used for ablation were 63.9 mW and 0.1 s, respectively. High-intensity plasma radiation was observed just after the laser irradiation. About 1 s after the plasma radiation, the strong CARS signal region appeared at the disrupted site, which then decreased exponentially with a timeconstant of 23.8 s. The CARS intensity depends on the molecular density of lipids and the phase matching capability of the complex structure of fused lipid vesicles in the focal volume. The result therefore indicates the decrease of the molecular density of lipids around the disrupted site and/or the structural change of the lipid vesicles with time after ablation.

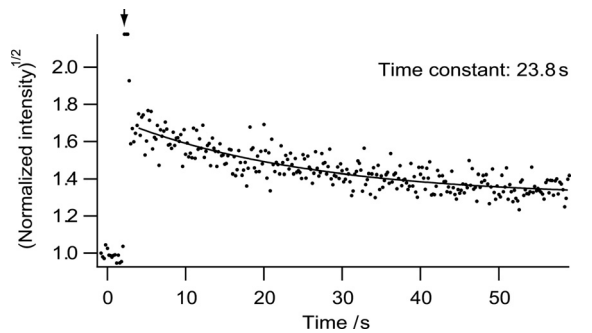

Fig. 3 Temporal behavior of the CARS signal at the laser-ablated site. The arrow indicates the time of laser irradiation. The CARS signal decreased exponentially with a time constant of 23.8 s.

Resealing of the cellular membrane occurs by patching the disrupted site with vesicles in the cytoplasm, as follows:[28] A few hundred vesicles in the cytoplasm accumulate at the disrupted site and are fused with each other, which are triggered by Ca^{2+} influx. The large united vesicles exocytotically fuse to the cellular membrane to seal the disrupted site. This process is well supported by our CARS measurements. The strong CARS signal around the disrupted site was observed only in the presence of Ca^{2+}, and the localized CARS signal increase around the disrupted site was detected with 3-D CARS imaging. The CARS signal decay after the disruption suggests the progression of vesicle fusion. The volume of a vesicle is proportional to cubic of the vesicle radius, but the surface area is proportional to the square of the vesicle radius. The surface area is fixed with the amount of lipids. Therefore, by fusion of the vesicles, the density of lipids will decrease. The vesicles also exocitotically fuse with the cellular membrane. These phenomena will reduce the lipid density in the focal volume around the disrupted site. Besides, the CARS signal behavior also includes the structural property of lipid vesicles in focal volume because of the change of the phase-matching capability. In the repair process, the shape of the vesicles changes by fusing with each other. The membrane repair is performed with the changes of density and structure of lipid vesicles. The decay of the CARS signal therefore indicates the spatiotemporal progression of patch vesicles.

Vesicles for membrane resealing are mainly recruited via motor proteins, such as myosin and kinesin. Myosin and kinesin move along actin filaments and microtubules with vesicles, respectively. It is known that the first response of resealing is mediated by myosin-dependent vesicle transportation.[29] In our CARS experiment, the rise time of the CARS signal after membrane disruption was <1 s (Fig. 3) because the CARS signal just after the laser ablation was hidden by the plasma radiation. The reported speed of the myosin-mediated vesicle transportation was about 1–3.5 μm/s.[29,30] Higher speed unknown vesicle transportation process was also suggested.[29] The observed area of Fig. 3 was near the plasma membrane because the axial resolution was $\sim$1.6 μm. The fast response via myosin that existed near the plasma membrane might be detected. To discuss the rise of the CARS signal, more high-speed imaging and optical filtering to remove the plasma radiation will be required.

4 Conclusion

In conclusion, we have demonstrated real-time CARS imaging of membrane disruption of a living HeLa cell induced by near-infrared laser ablation. In general, fluorescence microscopy is used to observe the distribution of vesicles in the resealing process.[28,31,32] However, accurate evaluation of the vesicle distribution is difficult because fluorescence microscopy involves the problems of photobleaching and the difficulty of staining the entire vesicles in a living cell. An electron microscope, such as an SEM or TEM, visualizes the nanometer-scale structure of vesicles.[33,34] However, fixation and dehydration processes required for electron microscopy prevent real-time observation of lipid dynamics. Fortunately, because there is no photobleaching in CARS measurement and a CARS signal is generated via intrinsic molecular vibrations of lipids; CARS imaging can de-

tect the distribution of lipids, which are difficult to stain with fluorophores. The real-time imaging of the resealing process by multifocus CARS microscopy allows us to monitor not only the lipid distribution at a disrupted site but also the lipid dynamics of the resealed vesicles.

We focused on lipid imaging of a cell in this study, but CARS imaging enables us to observe other molecular distributions, such as proteins and structural changes of molecules in cells and tissues by spectral analysis. We expect that this noncontact, optical imaging, and manipulation technique will open the door for revealing the nature of cells and for real-time diagnosis and surgery in medical applications.

Acknowledgment

This work was partially supported by a Grant-in-Aid for Scientific Research from the Ministry of Education, Culture, Sports, Science and Technology and the Development of Systems and Technology for Advanced Measurement and Analysis (SENTAN) program from the Japan Science and Technology Agency. One of the authors (T. M.) acknowledges support by Grant-in-Aid for JSPS Fellows from the Japan Society for the Promotion of Science (JSPS). The authors thank Dr. Y. Harada and Prof. T. Takamatsu (Kyoto Prefecture University of Medicine, Kyoto, Japan) for kindly providing the HeLa cells.

References

1. K. König, I. Riemann, P. Fischer, and K.-J. Halbhuber, "Intracellular nanosurgery with near infrared femtosecond laser pulses," *Cell. Mol. Biol.* **45**, 195–201 (1999).
2. N. I. Smith, K. Fujita, T. Kaneko, K. Katoh, O. Nakamura, and T. T. S. kawata, "Generation of calcium waves in living cells by pulsed-laser-induced photodisruption," *Appl. Phys. Lett.* **79**, 1208–1210 (2001).
3. D. G. Jay, "Selective destruction of protein function by chromophore-assisted laser inactivation," *Proc. Natl. Acad. Sci. USA* **85**, 5454–5458 (1988).
4. T. Tanabe, M. Oyamada, K. Fujita, P. Dai, H. Tanaka, and T. Takamatsu, "Multiphoton excitation-evoked chromophore-assisted laser inactivation using green fluorescent protein," *Nat. Methods* **2**, 503–505 (2005).
5. T. Shimada, W. Watanabe, S. Matsunaga, T. Higashim, H. Ishii, K. Fukui, K. Isobe, and K. Itoh, "Intracellular disruption of mitochondria in a living hela cell with a 76-MHz femtosecond laser oscillator," *Opt. Express* **24**, 9869–9880 (2005).
6. V. Kohli, A. Y. Elezzabi, and J. P. Acker, "Cell nanosurgery using ultrashort (femtosecond) laser pulses: applications to membrane surgery and cell isolation," *Laser Surg. Med.* **37**, 227–230 (2005).
7. A. Ashkin, J. M. Dziedzic, and T. Yamane, "Optical trapping and manipulation of single cells using infrared laser beams," *Nature* **330**, 769–771 (1987).
8. K. Svoboda, C. F. Schmidt, B. J. Schnapp, and S. M. Block, "Direct observation of kinesin stepping by optical trapping interferometry," *Nature* **365**, 721–727 (1993).
9. J. Ando, B. G, I. S. N, K. Fujita, and V. R. Daria, "Optical trapping and surgery of living yeast cells using a single laser," *Rev. Sci. Instrum.* **79**, 103705 (2008).
10. A. Heisterkamp, I. Z. Maxwell, J. M. U. E. Mazur, J. A. Nickerson, S. Kumar, and D. E. Ingber, "Pulse energy dependence of subcellular dissection by femtosecond laser pulses," *Opt. Express* **13**, 3690–3696 (2005).
11. H. Niioka, N. I. Smith, K. Fujita, Y. Inouye, and S. Kawata, "Femtosecond laser nano-ablation in fixed and non-fixed cultured cells," *Opt. Express* **16**, 14476–14495 (2008).
12. A. Khodjakov, R. W. Cole, and C. L. Rieder, "A synergy of technologies: combining laser microsurgery with green fluorescent protein tagging," *Cell Motil. Cytoskeleton* **38**, 311–317 (1997).
13. V. Gomez-Godinez, N. M. Wakida, A. S. Dvornikov, K. Yokomori, and M. W. Berns, "Recruitment of DNA damage recognition and repair pathway proteins following near-IR femtosecond laser irradiation of cells," *J. Biomed. Opt.* **12**, 054016 (2007).
14. N. M. Wakida, C. S. Lee, E. T. Botvinick, L. Z. Shi, A. Dvornikov, and M. W. Berns, "Laser nanosurgery of single microtubules reveals location-dependent depolymerization rates," *J. Biomed. Opt.* **12**, 024022 (2007).
15. A. Zumbusch, G. R. Holtom, and X. S. Xie, "Three-dimensional vibrational imaging by coherent anti-Stokes Raman scattering," *Phs. Rev. Lett.* **82**, 4142–4145 (1999).
16. M. Hashimoto, T. Araki, and S. Kawata, "Molecular vibration imaging in the fingerprint region by use of coherent anti-Stokes Raman scattering microscopy with a collinear configuration," *Opt. Lett.* **25**, 1768–1770 (2000).
17. X. Nan, J. Cheng, and X. S. Xie, "Vibrational imaging of lipid droplets in live fibroblast cells with coherent anti-Stokes Raman scattering microscopy," *J. Lipid Res.* **44**, 2202–2208 (2003).
18. X. S. Xie, J. Yu, and W. Y. Yang, "Living cells as test tubes," *Science* **312**, 228–230 (2006).
19. X. Nan, E. O. Potma, and X. S. Xie, "Nonperturbative chemical imaging of organelle transport in living cells with coherent anti-Stokes Raman scattering microscopy," *Biophys. J.* **91**, 728–735 (2006).
20. H. Kano and H. Hamaguchi, " Supercontinuum dynamically visualizes a dividing single cell, " *Anal. Chem.* **79**, 8967–8973 (2007).
21. C. L. Evans, E. O. Potma, M. Puoris'haag, D. Côté, C. P. Lin, and X. S. Xie, "Chemical imaging of tissue in vivo with video-rate coherent anti-Stokes Raman scattering microscopy," *Proc. Natl. Aca. Sci. USA* **102**, 16807–16812 (2005).
22. T. Minamikawa, M. Hashimoto, K. Fujita, S. Kawata, and T. Araki, "Multi-focus excitation coherent anti-Stokes Raman scattering (CARS) microscopy and its applications for real-time imaging," *Opt. Express* **17**, 9526–9536 (2009).
23. T. Minamikawa, H. Niioka, T. Araki, and M. Hashimoto, "Real-time molecular imaging of organelles in living cell by multifocus excitation CARS microscope," *Proc. SPIE* **7569**, 756927 (2010).
24. T. Minamikawa, N. Tanimoto, M. Hashimoto, T. Araki, M. Kobayashi, K. Fujita, and S. Kawata, "Jitter reduction of two synchronized picosecond mode-locked lasers using balanced cross-correlator with two-photon detectors," *Appl. Phys. Lett.* **89**, 191101 (2006).
25. M. Hashimoto, T. Asada, T. Araki, Y. Inouye, and S. Kawata, "Automatic pulse duration control of picosecond laser using two-photon absorption detector," *Jpn. J. Appl. Phys.* **44**, 3958–3961 (2005).
26. A. Vogel, J. Noack, G. Huttman, and G. Paltauf, "Mechanisms of femtosecond laser nanosurgery of cells and tissues," *Appl. Phys. B* **81**, 1015–1047 (2005).
27. A. Fein and M. Terasaki, "Rapid increase in plasma membrane chloride permeability during wound resealing in starfish oocytes," *J. Gen. Physiol.* **126**, 151–159 (2005).
28. P. L. McNeil and T. Kirchhausen, "An emergency response team for membrane repair," *Nat. Rev. Mol. Cell Biol.* **81**, 499–505 (2005).
29. G. Bi, R. L. Morris, L. G, J. M. Alderton, J. M. Scholey, and R. A. Steinhardt, "Kinesin- and myosin-driven steps of vesicle recruitment for Ca^{2+}-regulated exocytosis," *J. Cell. Biol.* **138**, 999–1008 (1997).
30. D. H. Schott, R. N. Collins, and A. Bretscher, "Secretory vesicle transport velocity in living cells depends on the myosin-v lever arm length," *J. Cell Biol.* **156**, 35–39 (2002).
31. C. S. Eddleman, M. L. Ballinger, M. E. Smyers, H. M. Fishman, and G. D. Bittner, "Endocytotic formation of vesicles and other membranous structures induced by Ca^{2+} and axolemmal injury," *J. Neurosci.* **18**, 4029–4041 (1998).
32. P. L. McNeil, K. Miyake, and S. S. Vogel, "The endomembrane requirement for cell surface repair," *Proc. Nat. Acad. Sci. USA* **100**, 4592–4597 (2003).
33. K. Miyake and P. L. McNeil, "Vesicle accumulation and exocytosis at sites of plasma membrane disruption," *J. Cell Biol.* **131**, 1737–1745 (1995).
34. P. L. McNeil and M. M. Baker, "Cell surface events during resealing visualized by scanning-electron microscopy," *Cell Tissue Res.* **304**, 141–146 (2001).